The Influence of Pr and Nd Substitution on Hydrogen Storage Properties of Mechanically Alloyed (La,Mg)$_2$Ni$_7$-Type Alloys

M. Balcerzak (iD)*, M. Nowak, and M. Jurczyk*

The (La,Mg)$_2$Ni$_7$-type alloys are candidates for hydrogen storage materials. In this study, mechanical alloying with subsequent annealing under the argon atmosphere at 1123 K for 0.5 h is applied to produce La$_{1.5-x}$Pr$_x$Mg$_{0.5}$Ni$_7$ and La$_{1.5-x}$Nd$_x$Mg$_{0.5}$Ni$_7$ alloys ($x = 0, 0.25, 0.5, 1$). A shaker-type ball mill is used in the study. The objective of the present study is to investigate the influence of the amount of Pr or Nd in the La-Mg-Ni alloy on the electrochemical, hydrogenation and dehydrogenation properties of (La,Mg)$_2$Ni$_7$-type materials. The x-ray diffraction analysis reveals the formation of multi-phase structure materials. The obtained alloys were studied by a conventional Sievert's type apparatus at 303 K. It has been observed that a chemical modification by Pr and Nd can affect the kinetics of the hydrogen absorption process and the maximum hydrogen storage capacity. Moreover, the stability of the electrochemical discharge capacity during cyclic work of the (La,Mg)$_2$Ni$_7$-type alloys is improved by a substitution with the La by Pr or Nd atoms.

1. Introduction

The La$_2$Ni$_7$ intermetallic alloy of a superstacking structure (1:1 LaNi$_5$ to LaNi$_2$ slabs ratio) is characterized by greater H-uptake than the LaNi$_5$ phase. Therefore, it is attractive for hydrogen storage systems and for secondary Ni-MH$_x$ batteries as negative electrode materials (Ref 1, 2). However, the practical use of this phase is limited due to several factors such as poor cycle stability of the electrochemical discharge capacity during the charging/discharging process.

There are several methods to improve the performance of hydrogen storage alloys, one of which is chemical modification. This approach is based on the fact that the final hydrogen storage properties of materials are directly related to the crystallographic structure and phase composition. It was revealed in the past that apartial substitution of the A and/or B atoms in A$_2$B$_7$-type materials by rare earth and/or transition metals can affect their structure and phase composition and therefore improve the cycling stability, the diffusion rate, the maximum hydrogen storage capacity, etc. (Ref 1, 3-5). For example, the effect of the Mg content on the properties of the La$_{2-x}$Mg$_x$Ni$_7$ system was investigated (Ref 6-8). The concentration of Mg in the basic system is very impactful on the final phase composition. It was shown that when $x = 0.48$-0.5,

$x = 0.6$ and $x > 0.48$, the following main phases (La,Mg)$_2$Ni$_7$, (La,Mg)Ni$_3$ and LaNi$_5$ were observed, respectively (Ref 7).

Moreover, the replacement of La by the Pr or Nd atoms in the La-Ni-based alloys can increase the hydrogen equilibrium pressure and improve the anti-corrosion ability (Ref 9-11). The La$_2$Ni$_7$-type materials chemically modified by Nd can be used as negative electrode materials in secondary Ni-MH$_x$ batteries characterized by an improved cyclic durability. These electrodes are characterized by an improved cyclic durability and can work below room temperature (233 K) (Ref 9). It is noteworthy that a partial substitution of La with the Pr atoms caused changes in the crystal structure of the A$_2$B$_7$ alloys. For example, in the La$_{0.8-x}$Nd$_x$Mg$_{0.2}$Ni$_{3.1}$Co$_{0.25}$Al$_{0.15}$ alloys, the phase abundance of the (La,Mg)$_2$Ni$_7$ phase decreases from 71.32 to 42.70 wt.%, while that of the LaNi$_5$ phase increases from 26.01 to 51.64 wt.% when x increases from 0 to 0.4 (Ref 12).

Among many methods of production of hydrogen storage materials, the La$_2$Ni$_7$-type alloys were mostly synthesized by conventional methods: vacuum magnetic levitation method (Ref 9), induction melting (Ref 1, 4, 10, 11, 13-15), melt spinning (Ref 16) or arc melting (Ref 2). However, still little is known about the La$_2$Ni$_7$-type alloys obtained by the mechanical alloying (MA) method, widely used in the past to obtain different types of non-equilibrium materials (Ref 3, 17). This process consists in repeated fracture, mixing and cold welding of a fine blend of elemental particles resulting in a size reduction and chemical reactions (Ref 18). As a non-equilibrium processing method, MA can be used to produce large quantities of materials at a relatively low cost. Recent studies suggest that the kinetics of hydrogen absorption and desorption of the alloys synthesized by MA can be significantly improved for large specific surface areas and a short hydrogen diffusion distance (Ref 19).

For this reason, in this work, MA and heat treatment were used to prepare the La-Pr-Mg-Ni and La-Nd-Mg-Ni alloys. The effect of substituting La with Pr or Nd on the hydrogenation

M. Balcerzak, M. Nowak, and **M. Jurczyk**, Institute of Materials Science and Engineering, Poznań University of Technology, Jana Pawla II no 24, 61-138 Poznan, Poland. Contact e-mail: mateusz.balcerzak@put.poznan.pl.

and electrochemical properties of the La-Mg-Ni alloy has been presented and discussed. Moreover, it is noteworthy that in this work the authors focused on the effect of chemical modification in a simple La-Mg-Ni system [not complex as in previous works (Ref 9)]. The authors believe that the substitution of elements performed in simple systems can provide information on the accurate and direct impact of the La replacement with Pr and Nd on the hydrogen sorption and electrochemical properties of the $(La,Mg)_2Ni_7$-type materials.

2. Experimental Details

2.1 Chemicals

Applied commercial materials: La powder—grated from rod (Alfa Aesar, 99.9%), Mg powder (Alfa Aesar, 45 μm, 99.8%), Ni powder (Aldrich, 5 μm, 99.99%), Pr powder—grated from rod (Alfa Aesar, 99.1%), Nd powder—grated from rod (Alfa Aesar, 99.9%).

All electrochemical measurements were taken in deaerated 6 M KOH solution prepared from the KOH flakes and 18 MΩ cm^{-1} water.

2.2 Preparation of Materials

The $La_{1.5-x}Pr_xMg_{0.5}Ni_7$ and $La_{1.5-x}Nd_xMg_{0.5}Ni_7$ alloy powders ($x = 0$, 0.25, 0.5, 1) were prepared by the MA and annealing processes. The elemental powders were weighted, blended and poured into vials in a glove box filled with the argon atmosphere. Mechanical alloying lasted 48 h in all cases and was carried out in the argon atmosphere. The ratio of the weight of the hard steel balls (12 mm in diameter) to the weight of powder was 4.2:1.

A heat treatment of the obtained as-milled powder materials was carried out in a furnace at 1123 K for 0.5 h. This process was conducted in high-purity argon.

2.3 Structure and Morphology Characterization

The structure characterization of the obtained alloys was carried out to find a correlation between the structures of the alloys and their phase compositions with the observed hydrogenation and dehydrogenation characteristics.

A PANalytical Empyrean powder diffractometer (CuKα radiation, λ = 1.54056 Å) was used to investigate the phase compositions of the materials after synthesis. The XRD measurements were taken at a room temperature with a voltage and anode current of 45 kV and 40 mA, respectively. The XRD profiles were refined with the Rietveld method using the Maud software.

The microstructure morphology of the obtained materials was determined by scanning electron microscopy (SEM)—VEGA TS5135 TESCAN digital microscopy imaging.

2.4 Electrochemical Measurements

All synthesized samples with the addition of carbonyl nickel powder (10 wt.%) were used as negative electrodes in the Ni-MH$_x$ systems. It is noteworthy that in this paper, the discharge capacities have been presented per unit gram of the measured material. A detailed description of the electrochemical measurements was included in the authors' previous work (Ref 8). The cycle stability of the materials was evaluated by the

capacity retaining rate after 30th and 50th cycles: $R = (C_x/C_{max}) \times 100\%$, where the C_x and the C_{max} are discharge capacities at cycle x (30, 50) and maximum discharge capacity, respectively.

2.5 Pressure–Composition–Isotherm (PCI) Tests

The obtained La-Mg-Ni-type alloys were studied by a conventional Sievert's type PCI apparatus, Particulate Systems, HPVA-200 with a vacuum pump. The mass of the sample for each measurement run was approx. 0.6 g. Before the hydrogen sorption–desorption measurements, no activation method was used. All alloys were degassed under vacuum at 303 K for 1 h before the tests.

Firstly, three cycles of hydrogen absorption kinetics measurements were performed under the hydrogen pressure of 3 MPa at 303 K. These studies also provided information on the activation properties of these materials. Between the cycles, the alloys were degassed at 673 K. After the kinetic measurements, the degassed La-Mg-Ni-type materials were tested to obtain the pressure–composition–isotherm curves (at 303 K and under a hydrogen pressure range of up to approx. 7 MPa). A detailed description of the apparatus and the measurements has been presented in the authors' previous work (Ref 17).

2.6 DSC Measurements

All of the La-Mg-Ni-type materials after the PCT tests were tested by a TA DSC Q20 scanning calorimeter (DSC). The tests were performed up to 873 K, with the heating rate of 10 K/min in the argon atmosphere.

3. Results and Discussion

3.1 Morphology, Structure and Phase Compositions

Figure 1 presents the SEM images of the $La_{1.0}Pr_{0.5}Mg_{0.5}Ni_7$ alloy powders—one of the investigated $(La,Mg)_2Ni_7$-type alloys. All alloys are composed of irregular porous particles. Moreover, all materials are characterized by a bimodal particle size distribution. The size of the alloy particles varies approximately from 100 to 800 μm. The rest of the particles have a size lower than 10 μm. (Part of them are attached to the surface of the larger particles.)

The authors did not observe any significant differences between the morphologies of the studied samples. The grains refinement after the substitution of La with Pr reported by Zhang et al. (Ref 16) for the melt-spun A_2B_7-type alloys was not observed.

Figure 2 presents the XRD patterns of the $La_{1.5-x}Pr_xMg_{0.5}Ni_7$ and $La_{1.5-x}Nd_xMg_{0.5}Ni_7$ alloy powders ($x = 0$, 0.25, 0.5, 1) after 48 h of MA and an additional heat treatment at 1123 K for 0.5 h in high-purity argon. The most important data from the Rietveld refinement of the XRD patterns are presented in Table 1. Compared to the results reported by Xiangqian et al., the annealing process described in this paper appears to be more preferable. Alloys with the main $(La,Mg)_2Ni_7$-type phase are obtained after a heat treatment at lower temperatures. Moreover, the time of the heat treatment process is much shorter (Ref 9).

It can be easily seen that all of the samples had a multi-phase structure. The main phase in all alloys is the $(La,Mg)_2Ni_7$-type
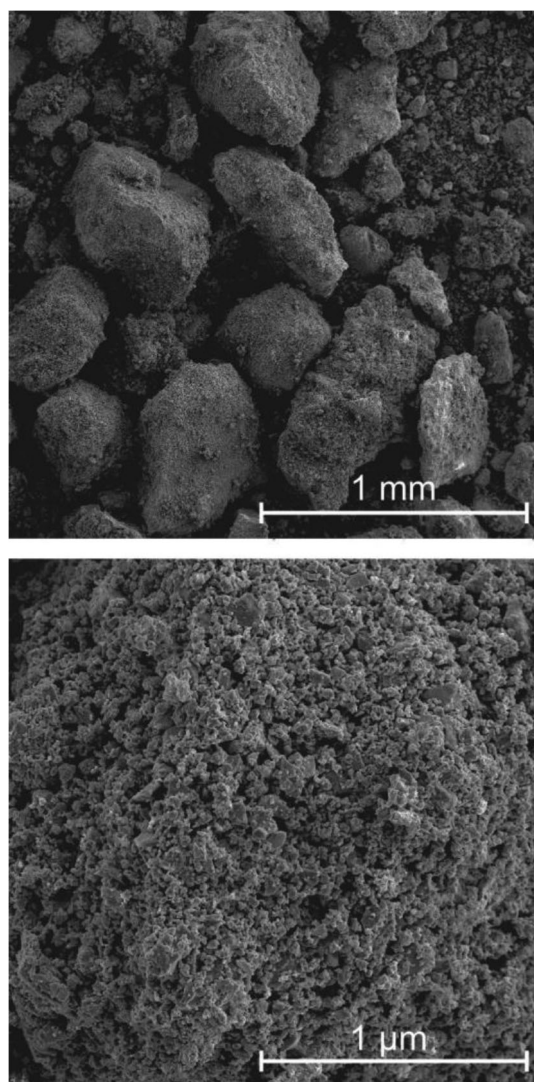
Fig. 1 SEM micrographs of $La_{1.0}Pr_{0.5}Mg_{0.5}Ni_7$ alloy obtained at different magnifications

one having a hexagonal structure crystallizing in the P63/mmc space group (Ce_2Ni_7-type)—marked in Fig. 2 and Table 1 as La_2Ni_7-type (H). The $(La,Mg)_2Ni_7$-type phase is obtained by stacking two AB_5 slabs with one A_2B_4 (Ref 1, 20). According to all the XRD patterns, no separate La, Pr, Nd, Mg or Ni elements were found.

In addition to the main $(La,Mg)_2Ni_7$-type phase, the unmodified $La_{1.5}Mg_{0.5}Ni_7$ alloy is composed of two minor phases. The first one is the $LaNi_5$-type phase having a hexagonal structure crystallizing in the P6/mmm space group ($CaCu_5$-type). The second one is the rhombohedral $(La,Mg)_2 Ni_7$-type phase crystallizing in the R-3 m space group—marked in Fig. 2 and Table 1 as La_2Ni_7-type (R). The same phase composition was obtained by Li et al. (Ref 1) for inductive melted $La_{0.60}R_{0.20}Mg_{0.20}(NiCoMnAl)_{3.5}$ alloys (R = La, Ce, Pr, Nd). However, the phase abundances are different than those presented in Table 1, which most likely results from different chemical compositions.

A partial substitution of La by the Pr atoms caused changes in the crystal structure of the alloys. The rhombohedral $(La,Mg)_2Ni_7$-type phase is replaced with the $LaNi_3$-type phase

that crystallizes in the same space group (R-3 m). The phase abundance of the main hexagonal $(La,Mg)_2Ni_7$-type phase increased, while the $LaNi_3$-type phase decreased with increasing Pr content in the material. Moreover, the $LaNi_3$-type phase is replaced by the $PrMgNi_4$-type phase in $La_{0.5}PrMg_{0.5}Ni_7$. The phase abundance of the $LaNi_5$-type phase remains at the same level (1-2 wt.%) regardless of the Pr content in the alloy.

The lattice parameters of all the $(La,Mg)_2Ni_7$-type, $LaNi_5$-type and $LaNi_3$-type phases were reduced with increasing Pr content in the alloy. It is due to the smaller atomic radius of Pr (0.1828 nm) compared to La (0.1877 nm).

A partial substitution of La by the Nd atoms caused changes in the minor phase composition of the alloys. The $LaNi_5$-type and the rhombohedral $(La,Mg)_2Ni_7$-type phases forming the unmodified $La_{1.5}Mg_{0.5}Ni_7$ alloy are replaced by the La_5Ni_{19}-type phase in the Nd-containing alloys. It is noteworthy that the La_5Ni_{19} theoretical hydrogen storage capacity is lower than that of La_2Ni_7. On the other hand, this phase is characterized by good catalytic properties (Ref 11). The phase abundance of the hexagonal $(La,Mg)_2Ni_7$-type phase increased, while the La_5Ni_{19}-type phase decreased with the increasing Nd content in the $La_{1.5-x}Nd_xMg_{0.5}Ni$ material. Based on the XRD studies, we can conclude that the maximum content of the hexagonal La_2Ni_7-type phase is observed for the $La_{0.5}Nd_1Mg_{0.5}Ni_7$ alloy.

The lattice parameters of the hexagonal $(La,Mg)_2Ni_7$-type phase were firstly increased (for $La_{1.25}Nd_{0.25}Mg_{0.5}Ni_7$) and then decreased with increasing Nd content in the alloy. The authors think that the initial increase in the hexagonal $(La,Mg)_2Ni_7$-type phase lattice parameters was caused by the change of the phase compositions occurring after a partial substitution of La with the Nd atoms, as described above. As was shown, the $La_{1.5}Mg_{05}Ni_7$ alloy is composed of the hexagonal La_2Ni_7-type phase and two secondary phases. The authors think that until the material is partially composed of the secondary $LaNi_5$-type and/or rhombohedral La_2Ni_7-type phase, the chemical composition of the hexagonal La_2Ni_7-type is depleted in lanthanum. After a partial substitution of La with the Nd atoms, a change in the secondary phases was observed. This change could cause a release of some of the La atoms embedded in the structure of minor phases prior to chemical modification. After a partial substitution, these La atoms could be incorporated into the main phase taking up the other atoms' place in the structure, thus creating the La-richer hexagonal La_2Ni_7-type phase. Because La has the largest atomic radius among the used elements, an increase in the lattice parameter was observed. To prove this claim, however, additional high-quality structure measurements have to be taken.

The lattice parameters of the secondary La_5Ni_{19}-type phase decreased with increasing Nd content in the alloy. As in the case of Pr, it is caused by a smaller atomic radius of Nd (0.1821 nm) compared to La (0.1877 nm). The same phenomenon was observed in the past for Nd- and Pr-substituted La-Ni alloys (Ref 9, 14).

Because the chemical modification of $La_{1.5}Mg_{0.5}Ni_7$ by Pr and Nd affected the lattice parameters of all phases, it can be stated that the Pr and Nd atoms co-form all of these phases. According to the work of Liu et al. (Ref 11), it can be concluded that the Pr and Nd atoms co-form an $[AB_5]$ subunit instead of $[A_2B_4]$. However, when the $[AB_5]$ subunit of the superlattice phase is saturated (especially for Pr-rich and Nd-rich samples), the extra Pr and Nd can co-form other minor phases.
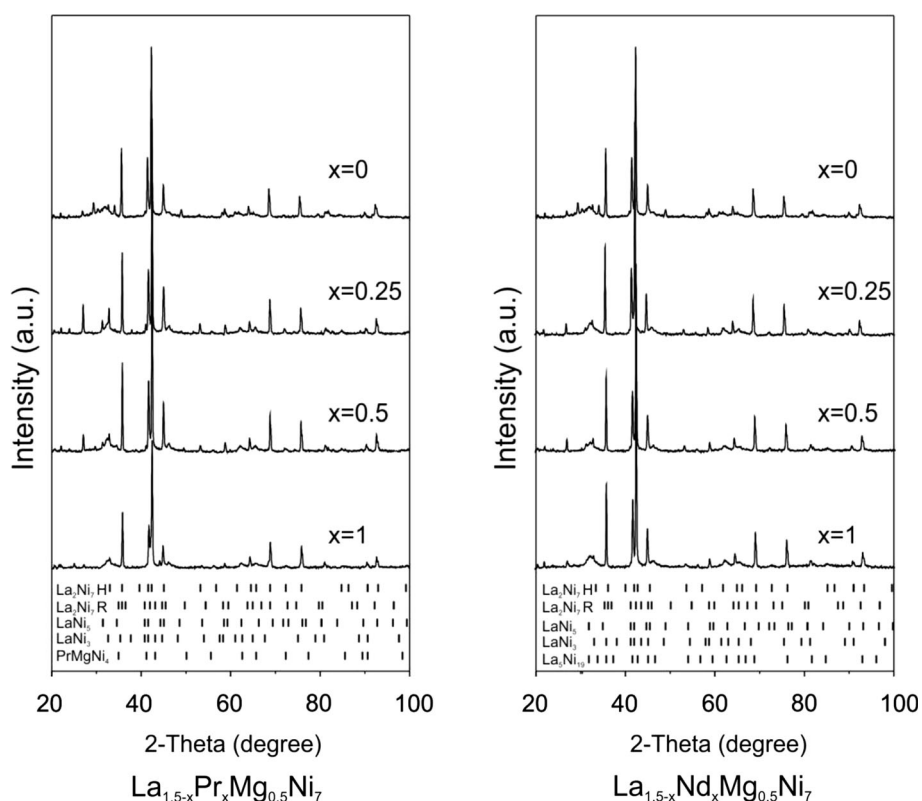
Fig. 2 XRD patterns of $La_{1.5-x}Pr_xMg_{0.5}Ni_7$ and $La_{1.5-x}Nd_xMg_{0.5}Ni_7$ alloys after 48 h of MA process and additional heat treatment

Table 1 Phase structures of the $La_{1.5-x}Pr_xMg_{0.5}Ni_7$ and $La_{1.5-x}Nd_xMg_{0.5}Ni_7$ alloys

Sample	Phase	Lattice parameter, Å		Phase abundance, wt.%
		a	*c*	
$La_{1.5}Mg_{0.5}Ni_7$				
$R_{wp} = 9.15$	La_2Ni_7-type (H)	5.0384	24.1457	89.98
$S = 1.94$	$LaNi_5$-type	5.2342	4.0629	1.81
	La_2Ni_7-type (R)	5.0336	36.2942	8.21
$La_{1.25}Pr_{0.25}Mg_{0.5}Ni_7$				
$R_{wp} = 9.34$	La_2Ni_7-type (H)	5.0182	24.1425	93.90
$S = 2.34$	$LaNi_5$-type	5.1678	3.9870	1.17
	$LaNi_3$-type	5.0862	25.0105	4.93
$LaPr_{0.5}Mg_{0.5}Ni_7$				
$R_{wp} = 9.49$	La_2Ni_7-type (H)	5.0146	24.1401	95.42
$S = 2.17$	$LaNi_5$-type	5.1601	3.9671	0.97
	$LaNi_3$-type	5.0830	24.9298	3.61
$La_{0.5}PrMg_{0.5}Ni_7$				
$R_{wp} = 9.33$	La_2Ni_7-type (H)	5.0059	24.1367	93.02
$S = 1.77$	$LaNi_5$-type	5.1589	3.9412	1.03
	$PrMgNi_4$-type	7.1016		5.95
$La_{1.25}Nd_{0.25}Mg_{0.5}Ni_7$				
$R_{wp} = 9.12$	La_2Ni_7-type (H)	5.0336	24.2519	95.54
$S = 2.74$	La_5Ni_{19}-type	5.0655	48.5512	4.46
$LaNd_{0.5}Mg_{0.5}Ni_7$				
$R_{wp} = 9.65$	La_2Ni_7-type (H)	5.0176	24.1549	96.77
$S = 2.33$	La_5Ni_{19}-type	5.0556	48.3706	3.23
$La_{0.5}NdMg_{0.5}Ni_7$				
$R_{wp} = 9.35$	La_2Ni_7-type (H)	5.0006	24.1380	97.38
$S = 2.29$	La_5Ni_{19}-type	5.0283	48.2309	2.62

Phase compositions of the described $La_{1.5-x}Nd_xMg_{0.5}Ni_7$ alloys differ from the compositions obtained in the past for the melted $La_{0.8}Nd_xMg_{0.2}Ni_{3.1}Co_{0.25}Al_{0.15}$ samples (Ref 9). For these materials, instead of the La_5Ni_{19}-type minor phase, $LaNi_5$-type and $LaMgNi_4$-type phases were observed. It means that even a small chemical modification (in this case by the Co and Al atoms) can significantly affect the structure of the A_2B_7-type alloys (Ref 9).

Based on the above-described XRD studies, it can be concluded that the substitution of La by Pr and Nd did not affect the change of the major phase. The addition of Pr and Nd stabilizes and increases the hexagonal $(La,Mg)_2Ni_7$-type phase abundance (Ref 15).

3.2 Electrochemical Measurements

The results of the electrochemical measurements taken on the $La_{1.5-x}Pr_xMg_{0.5}Ni_7$ and $La_{1.5-x}Nd_xMg_{0.5}Ni_7$ alloys are presented in Fig. 3. Moreover, the most important data from the electrochemical measurements are summarized in Table 2.

All of the electrodes displayed the maximum capacity at the first five cycles. The activation properties result from the phase composition and lattice parameters of the material. Such good activation properties were also observed for other La-Ni-type alloys, which means that this could be a common property of the La_2Ni_7-type materials (Ref 1, 9, 10).

The maximum discharge capacity of the $La_{1.5}Mg_{0.5}Ni_7$ alloy chemically modified by Pr is firstly reduced (for $La_{1.25}Pr_{0.25}Mg_{0.5}Ni_7$) and then increased to reach 308 mAh/g for the $La_{0.5}PrMg_{0.5}Ni_7$ alloy. An opposite trend was observed for alloys modified by Nd. The more the Nd in the alloy, the lower the discharge capacity. The best maximum discharge capacity (311 mAh/g) was obtained for the $La_{1.25}Nd_{0.25}Mg_{0.5}Ni_7$ alloy characterized by the highest La_5Ni_{19}-type phase content. As was stated above, the La_5Ni_{19} phase is characterized by very good catalytic properties. Moreover, studies on the electrochemical performance of the A_2B_7-type single-phase La_3MgNi_{14} alloy revealed that both the $(La,Mg)_5Ni_{19}$ and the $LaNi_5$ phases have a catalytic effect on the fast discharge of the alloy (Ref 11).

The discharge capacities result from several factors such as phase composition and phase abundances. Moreover, the hydrogen uptake during charging is also strongly related to the cell volume of the main phase. A reduction of the cell volume may cause a decrease in the interstitial sites for hydrogen and thus reduce the discharge capacity. In this work,

the authors showed that the chemical modification of the $La_{1.5}Mg_{0.5}Ni_7$ alloy affects all the said factors: phase composition, phase abundances and cell volumes. The measured discharge capacities result from all of the factors, but the exact impact of each factor is unknown.

A substitution of the La by Pr or Nd elements resulted in increased cycle stability of the electrodes. The best cycle stability after 50 cycles was obtained for the alloys with the highest Pr and Nd content. After 50 cycles, the cycle stability of MA and annealed $La_{0.5}PrMg_{0.5}Ni_7$ and $La_{0.5}NdMg_{0.5}Ni_7$ reached 64 and 71%, respectively. As was shown in the past, a partial substitution of La with rare earth elements is an effective way to improve the cycle life and high rate dischargeability.

The discharge capacities of all the studied alloys were degraded with the charge/discharge cycles. Most often, it was due to the following reasons:

- formation of stable hydride phases. However, as shown below, the PCT curves—studied alloy hydrides are unstable and can be mostly desorbed at the room temperature.
- partial oxidation of the electrode material. The degradation of the discharge capacity in the studied materials can originate from the formation and thickening of the $Mg(OH)_2$ and $La(OH)_3$ surface layers, that hinder the electron and mass transfer and consume the active material (Ref 11, 21). Wu et al. observed that La and Mg in the La-Mg-Ni alloys can be oxidized after approx. 10 cycles of charging/discharging. La, however, can be oxidized easier $(La(OH)_3)$ than Mg in the KOH electrolyte $(Mg(OH)_2)$ (Ref 10). Recently, it has been demonstrated that the Nd and Pr addition suppresses the oxidation of hydrogen-absorbing alloys (Ref 4, 13).
- pulverization of alloy particles caused by expansion and contraction of the cell volume during hydrogenation and dehydrogenation (Ref 22). This process not only increases the contact resistance between the alloy particles but also exposes smaller particles to the corrosion/oxidation of alkaline electrolyte (Ref 11). It also accelerates the oxidation and diffusion of rare earth elements toward the surface. During the charge/discharge process, the rare earth elements tend to diffuse toward the surface of the alloys, and the disproportion is determined by the atom concentration, the melting point and the cell volume (Ref 1). The Nd substitution can suppress the oxidation of the elements
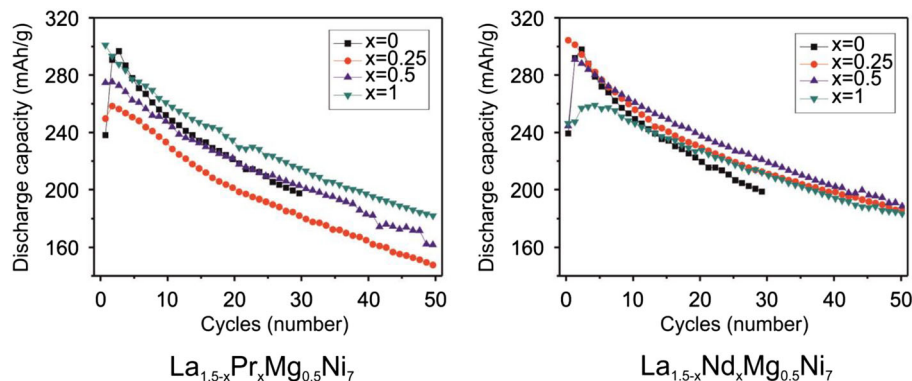
Fig. 3 Discharge capacities as a function of charging/discharging cycle number of electrodes prepared with $La_{1.5-x}Pr_xMg_{0.5}Ni_7$ and $La_{1.5-x}Nd_xMg_{0.5}Ni_7$ alloys

Table 2 Summarized data from electrochemical measurements on $La_{1.5-x}Pr_xMg_{0.5}Ni_7$ and $La_{1.5-x}Nd_xMg_{0.5}Ni_7$ alloys

Sample	$A_{\text{cycles-echem}}$	Maximum discharge capacity, mAh/g	Capacity retaining rate after 30th/50th cycle, %
$La_{1.5}Mg_{0.5}Ni_7$	3	304	67/$\cdots$
$La_{1.25}Pr_{0.25}Mg_{0.5}Ni_7$	2	265	71/58
$LaPr_{0.5}Mg_{0.5}Ni_7$	2	282	74/60
$La_{0.5}PrMg_{0.5}Ni_7$	1	308	72/64
$La_{1.25}Nd_{0.25}Mg_{0.5}Ni_7$	1	311	70/61
$LaNd_{0.5}Mg_{0.5}Ni_7$	2	297	76/65
$La_{0.5}NdMg_{0.5}Ni_7$	5	265	82/71

$A_{\text{cycles-echem}}$—number of activation cycles needed to obtain best electrochemical properties

Table 3 Summarized data from PCI and DSC measurements analyses on $La_{1.5-x}Pr_xMg_{0.5}Ni_7$ and $La_{1.5-x}Nd_xMg_{0.5}Ni_7$ alloys

Sample	A_{cycles}	H_{kin}, wt.%			T_{95}, min			$T_{\text{H-des}}$, K
		1 cycle	2 cycle	3 cycle	1 cycle	2 cycle	3 cycle	
$La_{1.5}Mg_{0.5}Ni_7$	2	1.60	1.59	1.59	301	13	13	404.2
$La_{1.25}Pr_{0.25}Mg_{0.5}Ni_7$	3	1.42	1.42	1.36	281	9	5	413.3
$LaPr_{0.5}Mg_{0.5}Ni_7$	1	1.47	1.29	1.38	10	86	51	423.7
$La_{0.5}PrMg_{0.5}Ni_7$	2	1.47	1.49	1.50	188	12	13	472.4
$La_{1.25}Nd_{0.25}Mg_{0.5}Ni_7$	2	1.53	1.49	1.48	101	4	5	519.2
$LaNd_{0.5}Mg_{0.5}Ni_7$	3	1.38	1.45	1.44	342	5	4	459.6
$La_{0.5}NdMg_{0.5}Ni_7$	2	1.38	1.40	1.39	252	4	11	429.2

H_{kin}—hydrogen concentration from kinetic measurements
T_{95}—time needed to reach 95% of maximum hydrogen capacity
A_{cycles}—number of activation cycles needed to obtain best kinetic properties
$T_{\text{H-des}}$ (°C)—hydrogen desorption peak temperature

due to its slower diffusion in materials caused by a much higher melting point (Ref 1). The influence of the pulverization effect apparently depends on the number of charging/discharging cycles.

Because the Nd and Pr addition suppresses the oxidation to the hydrogen-absorbing elements such as Mg and La, it can be concluded that the pulverization should be the dominant factor of the reduction of the discharge capacity (Ref 14). It is noteworthy that the cell volume expansion rate of the $LaNi_5$ phase is different from those of the superstacking phases—the discrete expansion leads to a serious pulverization and capacity degradation (Ref 11).

### 3.3 Hydrogen Absorption–Desorption Properties

Manometric, Sievert's type device was used to measure PCI and the kinetic properties of all the studied alloys. The most important data obtained from these studies are summarized in Table 3.

Figure 4 presents the time–capacity curves of the $La_{1.5-x}Pr_xMg_{0.5}Ni_7$ and $La_{1.5-x}Nd_xMg_{0.5}Ni_7$ alloys in the activation/kinetic measurements obtained at 303 K. These studies were conducted without any activation procedure. It can be seen that all of the alloys need to be activated before they obtain the best kinetic properties. Moreover, for most of the samples the hydrogenation process in the first cycle was initiated after some incubation time. (The only exception was the $LaPr_{0.5}Mg_{0.5}Ni$ alloy.) In the following cycles, the hydrogen sorption started immediately after filling the reaction chamber with hydrogen. The best hydrogenation properties were obtained in the second or third cycle. This means that all of the materials need to be activated. However, the process of activation is much easier compared to what described by Zhang et al. (Ref 15) described for inductive melted Pr-Mg-Ni alloys—those samples were four times hydrided (2 MPa, 1 h) and dehydrided (0.0001 MPa, 1 h) at 318 K.

The chemical substitution of La with Pr and Nd affected the kinetics of the hydrogen sorption. A partial replacement of La with the Nd atoms is effective in the reduction of time needed for the hydrogen absorption. Time needed to reach 95% of the maximum hydrogen capacity is reduced from 13 min for unmodified $La_{1.5}Mg_{0.5}Ni_7$ to 4-5 min for the Nd-containing alloys. Such good properties should be connected to the presence of the La_5Ni_{19}-type minor phase characterized by good catalytic properties.

The maximum hydrogen storage capacity strongly resulting from the structure and phase composition of the alloy was reduced after a chemical modification by Pr and Nd. This reduction is caused by the shrinkage of the cell volume caused by a partial substitution of La with the Pr and Nd atoms (Table 1). In smaller cells, the interstitial sites for hydrogen are smaller and the insertion of hydrogen is harder, thus leading to the reduction of the hydrogen storage capacity. The highest value was obtained for the unmodified $La_{1.5}Mg_{0.5}Ni_7$ alloy—1.6 wt.%.
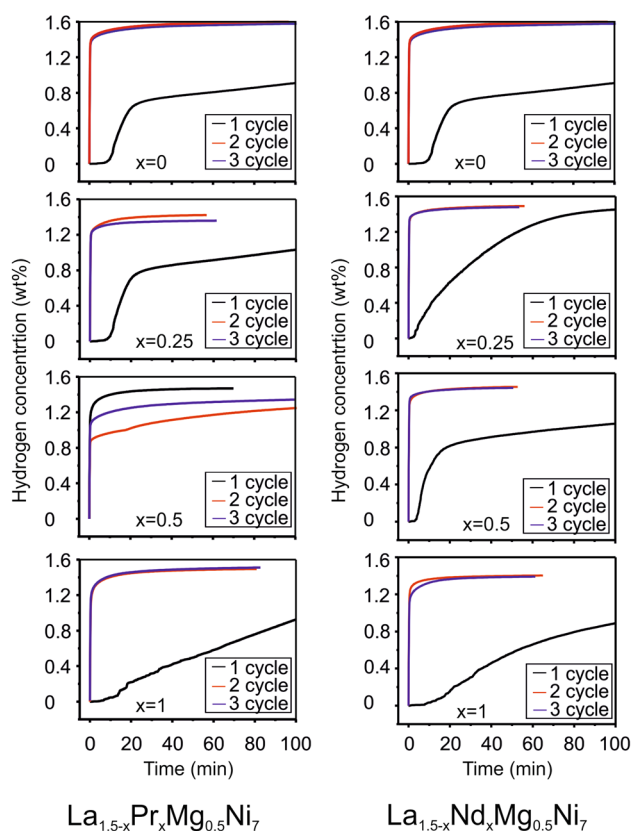
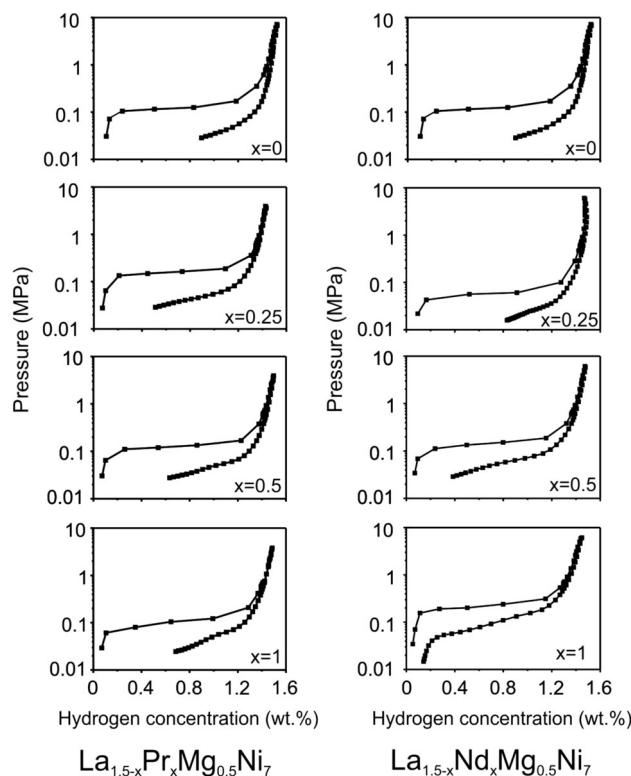**Fig. 4** Time–capacity curves of $La_{1.5-x}Pr_xMg_{0.5}Ni_7$ and $La_{1.5-x}Nd_xMg_{0.5}Ni_7$ alloys in activation/kinetic measurements

Fig. 5 PC isotherms at 303 K of $La_{1.5-x}Pr_xMg_{0.5}Ni_7$ and $La_{1.5-x}Nd_xMg_{0.5}Ni_7$ alloys

Figure 5 presents a comparison of the PCI curves obtained for all the studied alloys. These curves show that all materials actively absorb hydrogen at 303 K. For all samples, an absorption plateau region (which is very flat) was observed. This region corresponds to the transformation from the α-solid solution of hydrogen in the intermetallic alloy to the β-hydride phase. Despite the fact that the alloys are multi-phase, only one plateau region is visible for each sample. It is caused by a low secondary phase abundance. Moreover, the equilibrium pressures of the A_2B_7 and A_5B_{19} phases are very close due to their similar superstacking structures (Ref 11).

The plateau pressure heavily depends on the stability of the metal hydride, which results from the unit cell volume. It was previously shown that increasing the Mg content in the $La_{2-x}Mg_xNi_7$ alloy leads to an increase in the plateau pressure until it reaches the level of 10 MPa for $x = 1.0$ (Ref 14).

The plateau pressure (sorption process) observed on the PCT curves of the $La_{1.5-x}Pr_xMg_{0.5}Ni_7$ alloys increases with increasing Pr content in the sample, to reach the highest value for $La_{0.5}PrMg_{0.5}Ni_7$. This increase is related to the reduction of the cell volume—in smaller cells the interstitial sites for hydrogen are smaller and the insertion of hydrogen is harder. Therefore, the plateau pressure increases. The result is a decreased stability of the hydride phase. For $La_{0.5}PrMg_{0.5}Ni_7$, a decrease in the plateau pressure was observed—as caused by the change in the phase composition.

The chemical modification of the $(La,Mg)_2Ni_7$-type alloy by the Nd atoms also caused a change in the plateau pressure firstly decreased for $La_{1.25}Nd_{0.25}Mg_{0.5}Ni_7$ (caused by the

change in the phase composition—replacement of the $LaNi_5$-type and rhombohedral La_2Ni_7-type minor phases by the La_5Ni_{19}-type minor phase) and then increased with increasing content of the Nd atoms in the $La_{1.5-x}Nd_xMg_{0.5}Ni_7$ alloys. This increase was caused by the shrinkage of the cell volume (as was in the case of the modification by Pr described above).

The sorption plateau pressure for all of the studied samples has a level close to the atmospheric pressure, which is best in terms of their application. Due to the very low pressure of the desorption plateau for most of the samples, it is not possible to determine the reversibility of the hydriding–dehydriding process. (The low-pressure end of the plateau region is not visible.) Between the absorption and the desorption curves, a hysteresis appeared. It is most likely due to the transformation strains resulting from the cell volume expansion and the contraction (that cannot be relaxed) during the formation of hydrides formation and the decomposition.

The observed hysteresis can be used to predict the pulverization rate of the alloy during cycling. Alloys with a larger hysteresis have higher pulverization rates during the hydride/dehydride cycling (Ref 15).

All the materials after the PCI measurements were also studied by the DSC method—the obtained profiles are presented in Fig. 6. Additionally, the hydrogen desorption peak temperatures are listed in Table 3. All of the curves were characterized by one endothermic peak corresponding to the desorption of hydrogen from the alloys (hydrogen that was undesorbed during the PCI measurements). It can be seen that the hydrogen desorption peak temperature heavily depends on the phase composition. A partial substitution of La with Pr caused an increase in the hydrogen desorption peak tempera-
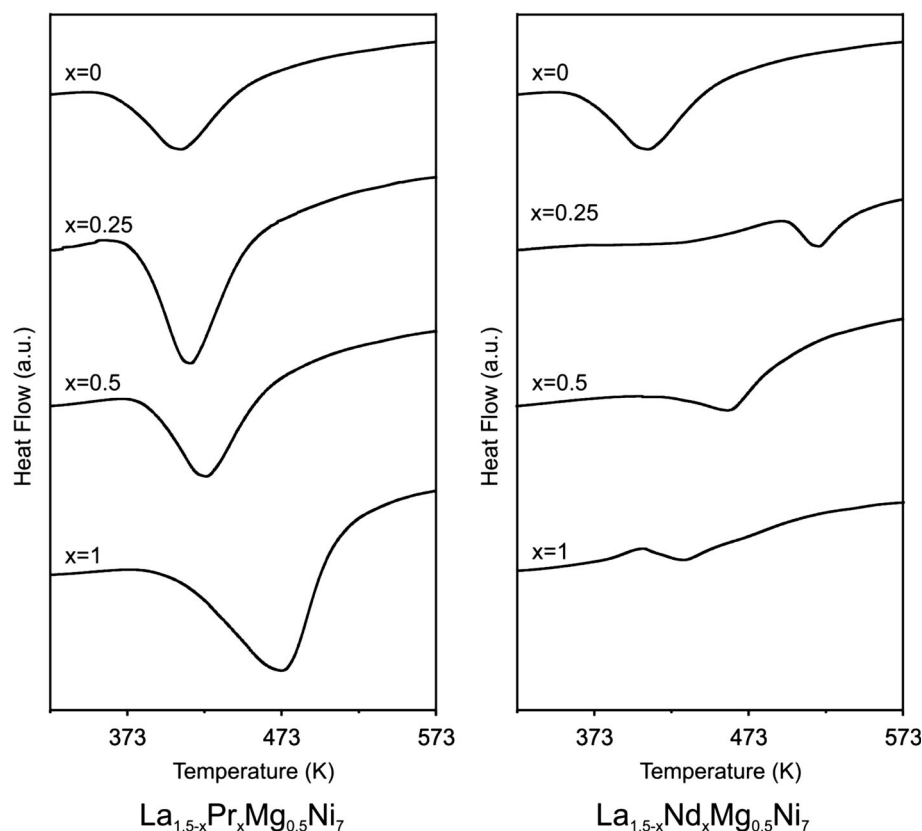
Fig. 6 DSC profiles of the hydrides of $La_{1.5-x}Pr_xMg_{0.5}Ni_7$ and $La_{1.5-x}Nd_xMg_{0.5}Ni_7$ alloys (after PCT tests)

ture. The hydride stability of the Nd-containing alloys increased with the higher content of the La_5Ni_{19}-type minor phase.

4. Conclusions

The $La_{1.5-x}Pr_xMg_{0.5}Ni_7$ and $La_{1.5-x}Nd_xMg_{0.5}Ni_7$ alloys ($x = 0, 0.25, 0.5, 1$) were effectively prepared by the MA and annealing processes. The structure, microstructure, electrochemical and hydrogen storage properties of these materials were carefully investigated.

The studies of the authors revealed that the substitution of La with Pr or Nd did not affect the change of the major phase—$(La,Mg)_2Ni_7$ is the main phase in all the studied alloys. The phase compositions of the studied alloys, however, depend on the content of the Pr or Nd atoms in the alloys.

It was clearly demonstrated that a partial substitution of La in $La_{1.5}Mg_{0.5}Ni_7$ can improve the electrochemical and hydrogen sorption properties of the $(La,Mg)_2Ni_7$-type system. The substitution of La with the Pr or Nd elements resulted in an increased cycle stability of the electrodes. The best cycle stability was obtained for the alloys with the highest Pr and Nd contents. Moreover, the chemical substitution of La with Pr or Nd also affected the kinetics of the hydrogen sorption and reduced the time of the hydrogenation process. The time needed to obtain 95% of the maximum hydrogen capacity at the 3rd cycle decreased to 4 min for the $LaNd_{0.5}Mg_{0.5}Ni_7$ alloy. The hydrogen sorption properties of the $(La,Mg)_2Ni_7$-type alloys presented in the paper are related to the changes in the crystal structure (cell volume) and phase composition of the materials.

References

1. Y. Li, D. Han, S. Han, X. Zhu, L. Hu, Z. Zhang et al., Effect of Rare Earth Elements on the Electrochemical Properties of La-Mg-Ni-Based Hydrogen Storage Alloys, *Int. J. Hydrogen Energy*, 2009, **34**, p 1399–1404
2. V.A. Yartys, A.B. Riabov, R.V. Denys, M. Sato, and R.G. Delaplane, Novel Intermetallic Hydrides, *J Alloys Compd.*, 2006, **408–412**, p 273–279
3. T. Huang, X. Yuan, J. Yu, Z. Wu, J. Han, G. Sun et al., Effect of Annealing Treatment and Partial Substitution of Cu for Co on Phase Composition and Hydrogen Storage Performance of $La_{0.7}Mg_{0.3}Ni_{3.2}Co_{0.35}$ Alloy, *Int. J. Hydrogen Energy*, 2012, **37**, p 1074–1079

4. T. Zhai, T. Yang, Z. Yuan, and Y. Zhang, An Investigation on Electrochemical and Gaseous Hydrogen Storage Performances of As-cast $La_{1-x}Pr_xMgNi_{3.6}Co_{0.4}$ (x = 0-0.4) Alloys, *J Hydrogen Energy*, 2014, **39**, p 14282–14287

5. T. Zhai, T. Yang, Z. Yuan, X. Sheng, W. Bu, Y. Qi et al., Influence of Hydrogen-Induced Amorphization and Annealing Treatment on Gaseous Hydrogen Storage Properties of $La_{1-x}Pr_xMgNi_{3.6}Co_{0.4}$ (x = 0-0.4) Alloys, *J Alloys Compd.*, 2016, **639**, p 15–20

6. X.G. Zhao and L.Q. Ma, Recent Progress in Hydrogen Storage Alloys for Nickel/Metal Hydride Secondary Batteries—Review, *Int. J. Hydrogen Energy*, 2009, **34**, p 4788–4796

7. L. Zhang, S. Han, Y. Li, S. Yang, X. Zhao, and J. Liu, Effect of Magnesium on the Crystal Transformation and Electrochemical Properties of A_2B_7-Type Metal Hydride Alloys, *J. Elektrochem. Soc.*, 2004, **161**, p A1844–A1850

8. M. Balcerzak, M. Nowak, and M. Jurczyk, Hydrogenation and Electrochemical Studies of La-Mg-Ni Alloys, *Int. J. Hydrogen Energy*, 2017, **42**, p 1436–1443

9. S. Xiangqian, C. Yungui, T. Mingda, W. Chaoling, D. Gang, and K. Zhenzhen, The Structure and 233 K Electrochemical Properties of $La_{0.8-x}Nd_xMg_{0.2}Ni_{3.1}Co_{0.25}Al_{0.15}$ (x = 0.0-0.4) Hydrogen Storage Alloys, *Int. J. Hydrogen Energy*, 2009, **34**, p 2661–2669

10. C. Wu, L. Zhang, J. Liu, Y. Li, S. Yang, B. Liu, and S. Han, Electrochemical Characteristics of $La_{0.59}Nd_{0.14}Mg_{0.27}Ni_{3.3}$ Alloy with Rhombohedral-Type and Hexagonal-Type A_2B_7 Phases, *J. Alloys Compd.*, 2017, **639**, p 573–581

11. J. Liu, S. Han, Y. Li, S. Yang, X. Chen, C. Wu, and C. Ma, Effect of Pr on Phase Structure and Cycling Stability of La-Mg-Ni-Based Alloys with A_2B_7- and A_5B_{19}-Type Superlattice Structures, *Electrochemica Acta*, 2015, **184**, p 257–263

12. S. Ma, M. Gao, R. Li, H. Pan, and Y. Lei, A Study on the Structural and Electrochemical Properties of $La_{0.7-x}Nd_xMg_{0.3}Ni_{2.45}Co_{0.75}Mn_{0.1}Al_{0.2}$ (x = 0.0-3.0) Hydrogen Storage Alloys, *J. Alloys Compd.*, 2008, **457**, p 457–464

13. J. Wang, S. Han, Y. Li, J. Liu, L. Che, L. Zhang, and J. Zhanf, Study of Phase Formation Mechanism and Electrochemical Properties of $La_{0.75-x}Nd_xMg_{0.25}Ni_{3.3}$ (x = 0, 0.15) Alloys Prepared by Powder Sintering, *J. Alloys Compd.*, 2014, **582**, p 552–557

14. V. Yartys and R. Denys, Structure-Properties Relationship in $RE_{3-x}Mg_xNi_9H_{10-13}$ (RE = La, Pr, Nd) Hydrides for Energy Storage, *J. Alloys Compd.*, 2015, **645**, p S412–S418

15. L. Zhang, W. Du, S. Han, Y. Li, S. Yang, Y. Zhao, C. Wu, and H. Mu, Study on Solid Solubility of Mg in $Pr_{3-x}Mg_xNi_9$ and Electrochemical Properties of $PuNi_3$-Type Single-Phase RE-Mg-Ni (RE = La, Pr, Nd) Hydrogen Storage Alloys, *Electrochemica Acta*, 2015, **173**, p 200–208

16. Y. Zhang, H. Ren, B. Li, S. Guo, Q. Wang, and X. Wang, Structures and Electrochemical Hydrogen Storage Behaviours of $La_{0.75-x}Pr_xMg_{0.25}Ni_{3.2}Co_{0.2}Al_{0.1}$ (x = 0-0.4) Alloys Prepared by Melt Spinning, *Int. J. Hydrogen Energy*, 2009, **34**, p 6335–6342

17. M. Balcerzak, J. Jakubowicz, T. Kachlicki, and M. Jurczyk, Hydrogenation Properties of Nanostructured Ti_2Ni-Based Alloys and Composites, *J. Power Sources*, 2015, **280**, p 435–445

18. M. Nowak and M. Jurczyk, Nanotechnology for the storage of hydrogen, *Nanotechnology for Energy Sustainability*, Vol 2, R. Baldev, M. Van de Voorde, and Y. Mahajan, Ed., Wiley, New York, 2017, p 433–458. ISBN: 978-3-527-34014-9

19. X. Ma, X. Xie, P. Liu, L. Xu, and T. Liu, Synerginc Catalytic Effect of Ti Hydride and Nb Nanoparticles for Improving Hydrogenation and Dehydrogenation Kinetics of Mg-Based Nanocomposite, *Prog. Nat. Sci. Mater. Int.*, 2017, **27**, p 99–104

20. H.L. Chu, S.J. Qui, Q.F. Tian, L.X. Sun, Y. Zhao, F. Xu et al., Effect of Ball-Milling Time on the Electrochemical Properties of La-Mg-Ni-Based Hydrogen Storage Composite Alloys, *Int. J. Hydrogen Energy*, 2007, **32**, p 4925–4932

21. M. Dornheim, S. Doppiu, G. Barkhordarian, U. Boesenberg, T. Klassen, O. Gutfleich et al., Hydrogen Storage in Magnesium-Based Hydrides and Hydride Composites, *Scr. Mater.*, 2017, **56**, p 841–846

22. F. Zhang, Y. Luo, D. Wang, R. Yan, L. Kang, and J. Chen, Structure and Electrochemical Properties of $La_{2-x}Mg_xNi7.0$ (x = 0.3-0.6) Hydrogen Storage Alloys, *J. Alloys Compd.*, 2007, **439**, p 181–188